7-1-2013

Structural and Magnetic Properties of $La_{0.7}Sr_{0.3}Mn_{1-x}Ni_xO_3$ ($x \leq 0.4$)

Thomas F. Creel

Jinbo Yang

Mehmet Kahveci

Satish K. Malik

et. al. For a complete list of authors, see http://scholarsmine.mst.edu/phys_facwork/740

Recommended Citation

T. F. Creel et al., "Structural and Magnetic Properties of $La_{0.7}Sr_{0.3}Mn_{1-x}Ni_xO_3$ ($x \leq 0.4$)," *Journal of Applied Physics*, vol. 114, no. 1, American Institute of Physics (AIP), Jul 2013.
The definitive version is available at http://dx.doi.org/10.1063/1.4810851

Structural and magnetic properties of $La_{0.7}Sr_{0.3}Mn_{1-x}Ni_xO_3$ ($x \leq 0.4$)

Thomas F. Creel,[1] Jinbo Yang,[2] Mehmet Kahveci,[3] Satish K. Malik,[4] S. Quezado,[4] O. A. Pringle,[1] William B. Yelon,[5] and William J. James[5]

[1]*Department of Physics, Missouri University of Science and Technology, Rolla, Missouri 65409-1170, USA*
[2]*State Key Laboratory for Artificial Microstructure and Mesoscopic Physics and School of Physics, Peking University, Beijing, China*
[3]*Department of Physics, University of Missouri, Columbia, Missouri, USA*
[4]*Departamento de Física Teórica e Experimental (DFTE), Universidade Federal do Rio Grande do Norte (UFRN), Natal, Brazil*
[5]*Department of Chemistry and Graduate Center for Materials Research, Missouri University of Science and Technology, Rolla, Missouri 65409-1170, USA*

(Received 5 January 2013; accepted 28 May 2013; published online 2 July 2013)

We have studied the structural and magnetic properties of $La_{0.7}Sr_{0.3}Mn_{1-x}Ni_xO_3$ ($x = 0.05$, 0.1, 0.20, 0.30, and 0.40) perovskites using x-ray and neutron diffraction and magnetic measurements. Our data consist of neutron ($\lambda = 1.479$ Å) and x-ray ($\lambda = 1.5481$ Å; Cu Kα) powder diffraction and magnetization measurements. We previously suggested these systems transition from ferromagnetic to antiferromagnetic ordering with the intermediate concentrations containing coexisting domains of ferromagnetically and antiferromagnetically ordered states. Upon further detailed examination, we find that the samples are homogeneous and that neutron data can be fitted to a single long-range magnetically ordered state. The compositional dependent changes are driven by a shift in the dominant near neighbor interaction from ferromagnetic to antiferromagnetic. In the intermediate compositions, peaks previously identified as due to antiferromagnetic ordering, in fact arise from charge ordering; the system remains in a ferromagnetic state where the Ni moments are antiparallel to the Mn moments. This interpretation supersedes multiphase and spin glass models for these complex systems. © *2013 AIP Publishing LLC*. [http://dx.doi.org/10.1063/1.4810851]

I. INTRODUCTION

Manganese-based perovskite materials continue to be of significant interest due to their wide ranging magnetic and electronic transport properties. From undoped $LaMnO_3$ to A-site doped $La_{1-x}Sr_xMnO_3$ to A-site and B-site doped $La_{1-x}Sr_xMn_{1-y}Z_yO_3$, these systems exhibit complex magnetic behavior, transitioning between ferromagnetic, paramagnetic, and antiferromagnetic phases with little or no change in the underlying crystallographic structure. These perovskites are known for the unusually large effect that an external magnetic field has on their ability to transport electricity and heat,[1,2] while other typical magnetic materials show little sensitivity to the same fields. Prior to the study of these perovskites, only very "clean" metals with a large electronic mean free path in zero field and metallic multilayers were found to show large field effects on transport properties.[1,3,4] Applications of these mixed-valence perovskites include cathodes for solid oxide fuel cells, magnetic storage devices, magnetoresistive read heads, catalysts and collosal magnetoresistance (CMR), and giant magnetoresistance (GMR) materials.[5–7] The magnetic and transport properties of these manganites have been described using double exchange, superexchange, semicovalent exchange, Jahn-Teller distortions, and electron-phonon coupling.[8–15]

$LaMnO_3$ is antiferromagnetically ordered at low temperatures ($T_N \sim 150$ K) and is a charge gap insulator due to the large correlation energy of the *d* electrons in the e_g band (d_z^2, $d_{x^2-y^2}$).[16,17] Charge neutrality dictates that all the Mn ions are in the 3+ state. Wollan and Koehler[3] were able to produce Mn^{4+} in $LaMnO_{3+\delta}$ by firing at different temperatures in an oxygen-rich environment. They produced up to 20% Mn^{4+} at an 1100 °C firing temperature in oxygen.

Upon replacing trivalent La^{3+} by divalent Sr^{2+}, Mn^{4+} is created as can be described by the formula $La^{3+}_{1-x}Sr^{2+}_x(Mn^{4+}_xMn^{3+}_{1-x})O^{2-}_3$. By substituting trivalent La^{3+} for divalent Sr^{2+} or Ca^{2+}, Wollan and Koehler[3] were able to increase the Mn^{4+} concentration. They found the Curie temperature (T_C) to be directly linked to the amount of Mn^{4+} present and samples with 30% Mn^{4+} exhibited almost pure ferromagnetic ordering with approximately the full predicted ferromagnetic moment per atom. For $x \sim 0.35$, their samples were purely ferromagnetic, whereas for $x < 0.25$ and $0.40 < x < 0.5$, their samples contained both ferromagnetic and antiferromagnetic phases.

Martin *et al.*[18] determined T_C for $La_{0.7}Sr_{0.3}MnO_3$ to be 378.1 K. The system is a ferromagnetic metal for temperatures $\leq$378.1 K with a magnetic moment per B-site of about 3.6 μ_β. Urushibara *et al.*[17] determined T_C for $La_{0.7}Sr_{0.3}MnO_3$ to be 369 K with a magnetic moment of 3.5 μ_β when prepared in a 50/50 mixture of O_2 and Ar. Their system was metallic for all temperatures. Both[17,18] magnetic moments are in good agreement with the calculated value of 3.7 μ_β/formula unit assuming complete spin alignment of the magnetic moments of the Mn ions, 4 μ_β for Mn^{3+} and 3 μ_β for Mn^{4+}. In the metallic region,[17,19–21] the dominant interaction between Mn^{3+} and Mn^{4+} is double exchange. For the other transition metal pairs, the superexchange mechanism is dominant and antiferromagnetic. A possible exception to this

rule is the Mn^{3+}-$O^{2-}$$Mn^{3+}$ superexchange interaction which may be either ferromagnetic or antiferromagnetic.[3]

While there is a body of research in the rare earth Ni-based perovskites ($RNiO_3$)[22] that find Ni to be in the Ni^{3+} low spin state, there has been little study of the Ni-substituted lanthanum-based perovskite, $La_{1-y}Sr_yMn_{1-x}Ni_xO_3$, where $0 \leq y \leq 0.3$ and $0 \leq x \leq 0.4$. There remains some ambiguity regarding the state of the Ni ion, whether it is Ni^{2+} or Ni^{3+}, whether the exchange interaction is ferromagnetic or antiferromagnetic, about the exchange mechanism (superexchange or double exchange) and the transport properties. In their study of $La_{0.67}Sr_{0.33}Mn_{1-x}Ni_xO_3$, Wang *et al.*[23] found Ni to be in the Ni^{2+} state citing x-ray spectroscopy but providing no data. They attributed their reduced volume and cell parameters to oxygen non-stoichiometry (Ni^{2+} is much larger than Mn^{3+}). They found for $x = 0.20$, a broad temperature transition from ferromagnetic to paramagnetic behavior in their magnetization measurements which they attributed to spin glass states. Further, they found the metal-to-insulator transition to occur between $x = 0.15$ and $x = 0.20$ with $x = 0.20$ to be completely insulating, and with increased Ni content, a reduction of T_C, cell parameters, volume and an increase in the temperature differences between T_C and the metal-to-insulator transition. In their study of $La_{0.70}Sr_{0.30}Mn_{1-x}Ni_xO_3$, Feng *et al.*[24] found the metal-to-insulator transition occurring at $x \sim 0.20$, with T_C and magnetization decreasing with increasing Ni content. They also found saturation magnetization values smaller than the calculated values assuming the Ni ion to be ferromagnetically coupled to the Mn ions. Wold *et al.*[25] found Ni ions in the Ni^{2+} and Ni^{3+} states in $LaMn_{1-y}Ni_yO_3$, with the Ni^{3+} in the low spin state with a ferromagnetic Ni^{3+}-$O^{2-}$$Mn^{3+}$ superexchange interaction.

A possible resolution to these contradictions is to assume that the dominant interaction controlling the nickel ordering is the antiferromagnetic interaction between Mn^{4+}-$O^{2-}$$Ni^{3+}$ rather than the ferromagnetic Ni^{3+}-$O^{2-}$$Mn^{3+}$ interaction. This interpretation arises from our neutron diffraction results and allows us to describe the magnetic behavior over the full compositional range.

In this study, we replace Mn in $La_{0.7}Sr_{0.3}MnO_3$ with up to 40% Ni and use neutron scattering, x-ray scattering and magnetic measurements to study the nuclear and magnetic structure and magnetic properties of the Ni-substituted perovskite. Neutron diffraction is uniquely appropriate to study the nuclear and magnetic structure of these perovskites due to the neutron magnetic scattering and the unique properties of the nuclear neutron scattering (including the negative Mn scattering length) which allows the crystal structure and the oxygen stoichiometry to be accurately determined. The possible oxidation states, electronic configuration, spin states, crystal radii, and ionic radii of our constituent elements are listed in Table I.[26] The ionic radii point towards Ni being in the low-spin Ni^{3+} state upon substitution of Ni for Mn in the perovskite structure.

TABLE I. Crystal and ionic radii from Shannon.[26]

Ion	Ox. state	Elec. config.	Coord. #	Spin state	Crystal rad (Å)	Ionic rad (Å)
La^{+3}	3	$4d^{10}$	6	…	1.172	1.032
Sr^{+2}	2	$4p^6$	6	…	1.320	1.18
O^{-2}	−2	$2p^6$	6	…	1.260	1.4
Mn^{+2}	2	$3d^5$	6	LS	0.810	0.67
Mn^{+2}	2	$3d^5$	6	HS	0.970	0.83
Mn^{+3}	3	$3d^4$	6	LS	0.720	0.58
Mn^{+3}	3	$3d^4$	6	HS	0.785	0.645
Mn^{+4}	4	$3d^3$	6	…	0.670	0.53
Mn^{+7}	7	$3p^6$	6	…	0.600	0.46
Ni^{+2}	2	$3d^8$	6	…	0.830	0.69
Ni^{+3}	3	$3d^7$	6	LS	0.700	0.56
Ni^{+3}	3	$3d^7$	6	HS	0.740	0.6
Ni^{+4}	4	$3d^6$	6	LS	0.620	0.48

II. EXPERIMENTAL

Polycrystalline samples of $La_{0.7}Sr_{0.3}Mn_{1-x}Ni_xO_3$ ($0 \leq x \leq 0.4$) were prepared using a conventional solid-state reaction method in air. Appropriate amounts of high purity La_2O_3, $SrCO_3$, MnO_2, and Ni_2O_3 powders were weighed and mixed according to the desired stoichiometry for each sample. The samples were ground using a high energy ball mill for 5 h, pressed into pellets at 10 000 psi and then fired at 1350 °C for 24 h in air with a room-air quench upon removal from the oven. After 24 h of cooling, the samples were re-ground, pressed, and fired using the same process.

Neutron-diffraction data were collected at the University of Missouri Research Reactor (MURR) facility using a position sensitive detector diffractometer with a neutron wavelength of $\lambda = 1.479$ Å. X-ray diffraction data were collected with an XPERT PRO diffractometer using a Cu Kα wavelength of $\lambda = 1.5481$ Å. Powder diffraction data were refined using the FULLPROF suite of programs.[27] Magnetic measurements were performed at the University of Brasilia, Brasilia DF, Brazil using a vibrating sample magnetometer and a Quantum Design Physical Property Measurement System with the AC magnetization option.

III. RESULTS AND DISCUSSION

In our previous work on $La_{0.7}Sr_{0.3}Mn_{1-x}Ni_xO_3$, (Ref. 28) we reported that the system crystallizes in the rhombohedral perovskite structure. At low nickel concentrations the system is a ferromagnetic metal, while at high concentrations the system is an antiferromagnetic insulator. In the intermediate regions, we previously reported the coexistence of two magnetic phases.

In this work, we provide a revised magnetic ordering schema based on further analysis of neutron-scattering data and magnetic measurements. At low Ni concentrations, the system is comprised of ferromagnetic layers (Figure 1(a)) with the Ni^{3+} moments aligned antiferromagnetically to the Mn^{3+} and Mn^{4+} moments, causing a net reduction in the measured ferromagnetic moments as before. However, with sufficient nickel, instead of random ferromagnetic and antiferromagnetic domains, charge ordering appears, leading to a ferromagnetic state with layers of unequal ferromagnetic moments (Figure 1(b)). At high nickel concentrations, the interaction between adjacent planes is antiferromagnetic

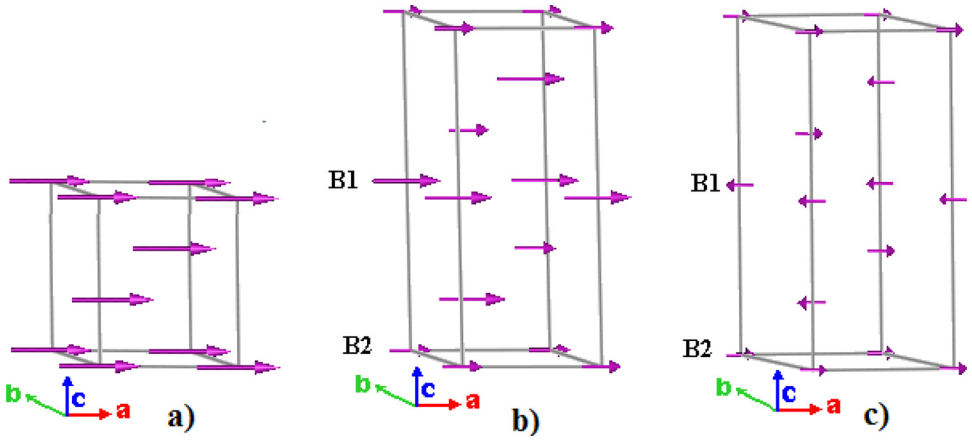

FIG. 1. Magnetic unit cells for the perovskite. Depicted magnetic unit cells are (a) ferromagnetic unit cell for 8% Ni, (b) the ferromagnetic (unequal moment magnitudes) doubled unit cell containing B1 and B2 layers for 21% Ni, and (c) the antiferromagnetic unit cell containing B1 and B2 layers for 31% Ni. The moment directions in the basal plane and labeling of B1 and B2 layers are arbitrary and chosen for convenience.

with the Mn^{4+} moments antiparallel to the Ni^{3+} and Mn^{3+} moments (Figure 1(c)). Only peaks identified as due to antiferromagnetic ordering are observed in the neutron-diffraction data. Peaks consistent with ferromagnetic and antiferromagnetic states are observed and fitted with a single phase model.

Refined neutron-diffraction data from the prepared stoichiometries of $x = 0.05$, 0.10, 0.20, 0.30, and 0.40 result in values of $x = 0.05$, 0.08, 0.16, 0.21, and 0.31 with the presence of 0.26%, 1.65%, 3.63%, 7.31%, and 8.89% of NiO impurity, respectively. The NiO percentages are derived from multiphase Rietveld refinements using the FULLPROF code. For the remainder of this discussion, we will refer to the refined stoichiometries. The neutron refinement results are presented in Table II. The atomic parameters (a, c, and volume) decrease with increasing Ni content while the oxygen stoichiometry changes very little. The decreasing cell parameters combined with the constant oxygen stoichiometry indicate Ni to be in the Ni^{3+} state. If Ni were in the Ni^{2+} state, one would expect the volume to increase, given stoichiometric oxygen.

Figure 2 shows the neutron diffraction data at 300 K subtracted from data collected at 12 K. This difference curve allows the elimination of all effects which are not temperature dependent. The large positive and negative swings for the (202), (006), and (024) reflections are due to temperature-driven shifts in lattice parameters, causing a shift in peak positions. Significant reductions in the ferromagnetic intensities occur between $x = 0.16$ and $x = 0.21$. The (012) and the combined (110) and (104) peaks contain both nuclear and ferromagnetic contributions to the intensities. The ferromagnetic contribution decreases steadily with increasing nickel content and disappears completely before $x = 0.31$. At $x = 0.31$, a peak associated with a doubling of the unit cell along the c-axis with indices (101 + 003) is clearly visible. In fact, this peak is barely visible at $x = 0.21$. The peaks not annotated are associated with the NiO phase.

At 12 K, ferromagnetic ordering is found for $0.05 \leq x \leq 0.16$. The refined moment on the manganese site decreases with increasing nickel content. The magnetic cell is pictured in Figure 1(a). At $x = 0.05$, a magnetic moment of 3.27 μ_β per B-site is obtained. This value is lower than that obtained for the parent perovskite $La_{0.7}Sr_{0.3}MnO_3$ where Martin and Shirane[18] find 3.6 μ_β per manganese site while Urushibara *et al.*[17] find 3.5 μ_β per manganese site in a reduced oxygen

TABLE II. Refined parameters: magnetic moment (μ_β), a, c, volume, and χ^2 versus refined Ni content from neutron-diffraction refinements. The magnetic moments are calculated on the Mn atom occupational sites and represent average magnetic moments per Mn site. The number in parenthesis represents the 1σ uncertainty in the last digit.

Ni content		0.05	0.08	0.16	0.21	0.31
12 K	$\mu_{B-1,\,Mn}(\mu_\beta)$	3.27 (2)	3.15 (2)	2.91 (2)	1.67 (9)	−1.09 (3)
	$\mu_{B-2,\,Mn}(\mu_\beta)$	3.27 (2)	3.15 (2)	2.91 (2)	2.59 (9)	1.09 (3)
	a (Å)	5.4941 (1)	5.4910 (1)	5.4831 (1)	5.4769 (2)	5.4650 (2)
	c (Å)	13.3110 (3)	13.3032 (3)	13.2841 (3)	13.2731 (5)	13.2511 (7)
	Cell vol $(Å)^3$	347.96 (1)	347.37 (1)	345.87 (1)	344.81 (2)	342.74 (2)
	Oxygen stoich	3.02 (2)	3.01 (2)	2.98 (2)	3.03 (3)	2.96 (3)
	χ^2	3.22	3.38	2.27	2.74	2.79
300 K	$\mu_{FM,\,Mn}(\mu_\beta)$	1.91 (3)	1.25 (4)	0.3 (2)	*n/a*	*n/a*
	$\mu_{AFM,\,Mn}(\mu_\beta)$	*n/a*	*n/a*	*n/a*	*n/a*	0.53 (6)
	a (Å)	5.5007 (1)	5.4988 (1)	5.4901 (1)	5.4821 (2)	5.4723 (2)
	c (Å)	13.3485 (4)	13.3435 (3)	13.3219 (4)	13.3121 (5)	13.2911 (7)
	Cell vol $(Å)^3$	349.78 (2)	349.41 (1)	347.75 (2)	346.48 (2)	344.69 (3)
	Oxgen stoich	3.02 (2)	3.01 (2)	2.98 (2)	3.03 (3)	2.96 (3)
	χ^2	2.80	2.56	2.27	2.88	2.97

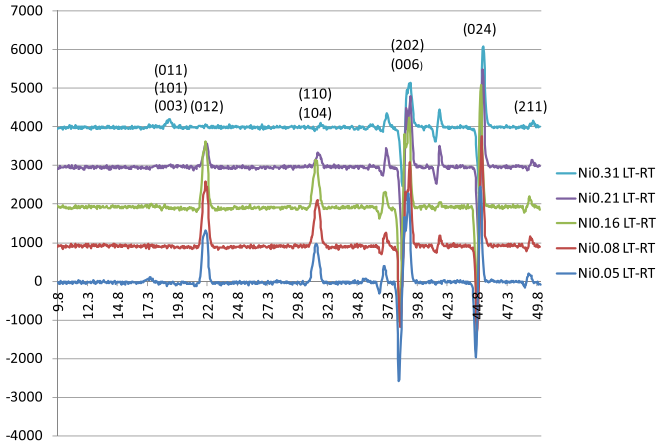

FIG. 2. Intensity versus scattering angle of neutron-scattering data collected at 300 K subtracted from data collected at 12 K for all Ni-substituted concentrations. Successive concentrations are offset by 200 counts.

atmosphere. This behavior points to an antiferromagnetic alignment between the Ni^{3+} and the ferromagnetically aligned Mn^{3+} and Mn^{4+} moments at low concentrations.

Magnetic moments for Mn^{3+} (4 μ_β) and Mn^{4+} (3 μ_β) are reliably known from a large body of works. However, the magnetic moment for the Ni^{3+} ion is not known in this system. To determine the Ni^{3+} magnetic moment, we fit a straight line to the net moment between $x = 0$ and $x = 0.16$ while accounting for the reduction of the Mn^{3+} concentration. For $x = 0$ (parent compound), we use the value of 3.6 μ_β from Martin *et al.*[18] For the remaining points, we use our refined values. This yields a Ni^{3+} moment of 1.54 μ_β in reasonable agreement with the 1.73 μ_β calculated by Goodenough and Loeb[14] for the Ni^{3+} square (dsp^2) covalent bond. It is closer to the 1 μ_β spin only value of low spin Ni^{3+} than the spin only value of 3 μ_β of high spin Ni^{3+}. The same results are seen in the $RNiO_3$.[22]

At 12 K for $x = 0.21$, in addition to the ferromagnetic intensity observed on the (012) and the combined (110) + (104) peaks, we observe the emergence of a very small peak comprised of the (101) and (003) reflections that is only present at low temperature, and therefore conclude that it is magnetic. This implies a doubling of the unit cell in which the B-site is split into B1 and B2 layers (Figure 1(b)). The insets in Figure 3 show the observed and fitted data using the best nuclear-only model. The misfits highlight the magnetic contributions. This was previously explained by using a two phase model consisting of a small antiferromagnetic component in a ferromagnetic matrix.[28] Upon further study, we find no evidence of phase separation in the neutron data; all the peak widths and shapes are consistent with a single phase material. If the system had separated into antiferromagnetic and ferromagnetic domains, we would expect to find different cell parameters yielding doubled peaks or causing peak broadening, if for no other reason than differing magnetostriction. Therefore, we looked for an alternative single phase model where all the magnetic scattering can be fit with a single magnetic phase. This was accomplished by considering a charge ordered state in which the unit cell is doubled along the c-axis (Figure 1(b), Table III). In this charge ordered state, all of the Mn^{4+} is assumed to be on the B2 layer, Ni^{3+} is distributed on both layers and Mn^{3+} accounts for the remaining sites on both layers.

This is the most highly ordered configuration we can achieve with these cations. The net charge on the B1 and B2 layers is −0.30 and +0.30, respectively. The intensity observed from the (101) and (003) reflections can be solved using a double unit cell along the c-axis, allowing the (0,0,0), (2/3,1/3,1/3), and (1/3,3/2,2/3) reflections to be estimated independently of the (0,0,1/2), (2/3,1/3,5/6), and (1/3,2/3,1/3) positions within the $P\bar{1}$ space group, yielding different average moments in the B1 and B2 layers with parallel alignment. The refined moments on the two layers

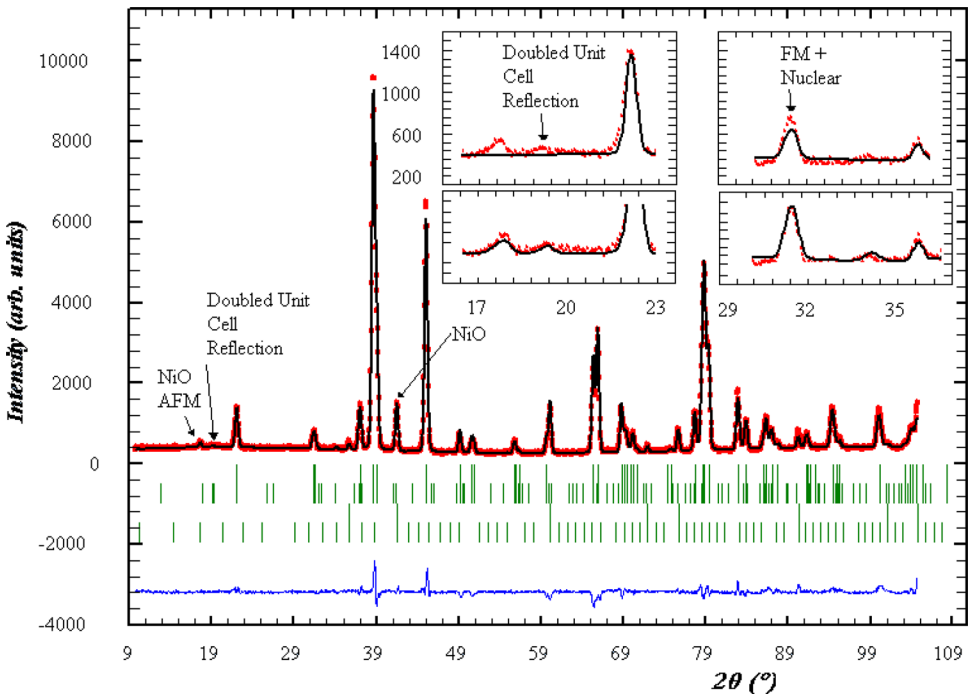

FIG. 3. Neutron-diffraction refinement of the $La_{0.7}Sr_{0.3}Mn_{0.79}Ni_{0.21}O_3$ sample at 12 K (refined stoichiometric Ni content). The reflection markers below the plot are, in order, nuclear perovskite structure, ferromagnetic perovskite structure, NiO nuclear structure, and AFM NiO structure. The insets show the magnified regions around the small magnetic peaks prior to magnetic refinement.

TABLE III. Calculated and refined magnetic moments (at 12 K) and charge neutrality calculation for all Ni concentrations. All columns except the last two present charge neutrality calculations, the last two columns contain calculated and refined magnetic moments using 1.54 μ_β for Ni.

Ni content	La + Sr – O net charge	%	Mn^{3+} net charge	%	Mn^{4+} net charge	%	Ni^{3+} net charge	Total net charge	Mag mom calc ($\mu\beta$)	Mag mom 12 K refined
Parent	−3.30	0.70	2.10	0.30	1.20	…	…	…	3.70	3.6[a]
0.05	−3.30	0.65	1.95	0.30	1.20	0.05	0.15	0.00	3.42	3.27
0.08	−3.30	0.62	1.86	0.30	1.20	0.08	0.24	0.00	3.26	3.15
0.16	−3.30	0.54	1.62	0.30	1.20	0.16	0.48	0.00	2.81	2.91
0.21-B1	−3.30	0.79	2.37	0.00	0.00	0.21	0.63	−0.30	2.84	2.59
0.21-B2	−3.30	0.19	0.57	0.60	2.40	0.21	0.63	0.30	2.24	1.67
0.31-B1	−3.30	0.39	1.17	0.30	1.20	0.31	0.93	0.00	1.14	1.09
0.31-B2	−3.30	0.39	1.17	0.30	1.20	0.31	0.93	0.00	−1.14	−1.09

[a]Note—value from Martin and Shirane.[19]

are 2.59 μ_B and 1.67 μ_B, in reasonable agreement with the moments calculated using our new model, 2.84 μ_B (calculation goes as 0.79*4 μ_B + 0*3 μ_B−0.21*1.54 μ_B) and 2.24 μ_B.

At 12 K for x = 0.31, we only find antiferromagnetic ordering. The magnetic cell is depicted in Figure 1(c). The fitted moment on the B-site is much lower than the moments observed in the lower-doped samples. The fitted moments can be modeled by assuming that the Ni^{3+} and Mn^{4+} moments are antiparallel, while the Mn^{3+} and Ni^{3+} moments are parallel. The magnetic layers are antiferromagnetically stacked, supporting a ferromagnetic superexchange between Mn^{3+} and Ni^{3+} and an antiferromagnetic superexchange between Mn^{4+} and Ni^{3+} with the latter being dominant. Agreement between observed and calculated moments is achieved assuming constant Mn^{3+}, Mn^{4+}, and Ni^{3+} moments at all x. This implies that the system is long range ordered, eliminating the need for spin glass or cluster models. The observed sharp diffraction peaks further support this conclusion.

The results are summarized in Table III which gives the charge distribution and magnetic moments assuming stoichiometric oxygen. Also included are the calculated magnetic moments using our new model described above, where the Ni magnetic moments align antiferromagnetically to the ferromagnetically aligned Mn moments for x < 0.31. At x = 0.31, the system orders antiferromagnetically.

The Curie temperature in the ferromagnetic region decreases steadily with increased Ni concentration and is less than 300 K at x = 0.21. At x = 0.31, the system is antiferromagnetic and T_N exceeds room temperature.

Magnetization measurements (Figure 4) indicate that T_C decreases with increasing Ni concentration. There are differences between the zero field-cooled versus field-cooled magnetization (M_{ZFC} and M_{FC}) below T_C for all samples. All samples except x = 0.05 exhibit antiferromagnetic-like behavior below 50 K. For x = 0.08 and x = 0.16, both M_{ZFC} and M_{FC} curves exhibit an antiferromagnetic-like transition at approximately 45 K that increases in intensity with increased nickel content. With the onset of charge ordering at x = 0.21, a distinctive antiferromagnetic-like transition at approximately 10 K is seen only in the M_{ZFC} curve. The differences between M_{ZFC} and M_{FC} curves have routinely been ascribed to spin glass, spin clusters or re-entrant spin glass.[23,24,29] However, we believe that these differences are actually due to charge ordering and the complex competition between the Ni^{3+}-O-Mn^{3+} ferromagnetic couplings and the Ni^{3+}-O-Mn^{4+} and Ni^{3+}-O-Ni^{3+} antiferromagnetic couplings. For x = 0.08 and 0.16, the applied magnetic field coerces a magnified magnetic response while at x = 0.21, it suppresses the weakly charge ordered state as was observed by Tomioka *et al.*[31] in the $Pr_{0.5}Sr_{0.5}MnO_3$ system.

The T_C's and the magnetic moments are in good agreement with those of Hu *et al.*[30] and Wang *et al.*[23] There is a significant separation between M_{ZFC} and M_{FC} curves for x = 0.16 to 0.21, indicating a likely metal to insulator transition as observed by Feng *et al.*[24] where they found this transition occurs near x = 0.20. In our model, the metal to insulator transition is also accompanied by charge ordering.

The M_{ZFC} and M_{FC} curves for x = 0.16 exhibit a broad ferromagnetic to paramagnetic transition, which may be an indication of the imminent onset of charge ordering and metal to insulator transition. The x = 0.16 M_{ZFC} curve exhibits a transition to an antiferromagnetic-like behavior below 50 K while the FC curve exhibits an antiferromagnetic-like behavior below 100 K that is a function of temperature. These M_{ZFC} and M_{FC} curves exhibit complex magnetic ordering in

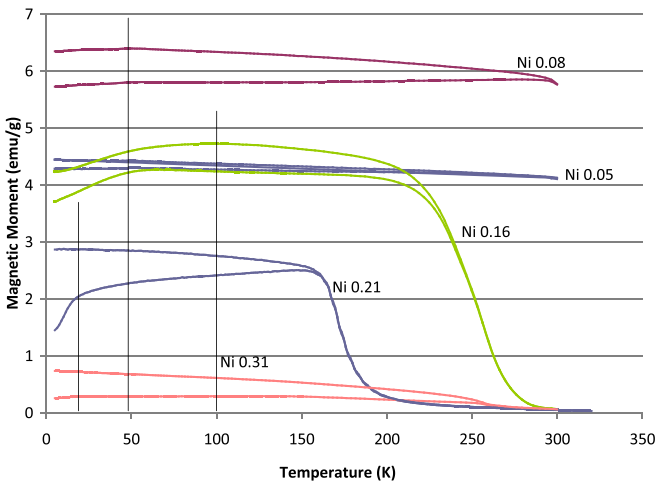

FIG. 4. ZFC and 100 Oe FC measurements of magnetization vs temperature for all nickel concentrations. For each sample, the ZFC is the lower while the FC is the upper segment of the curves. The vertical lines are to guide the eye.

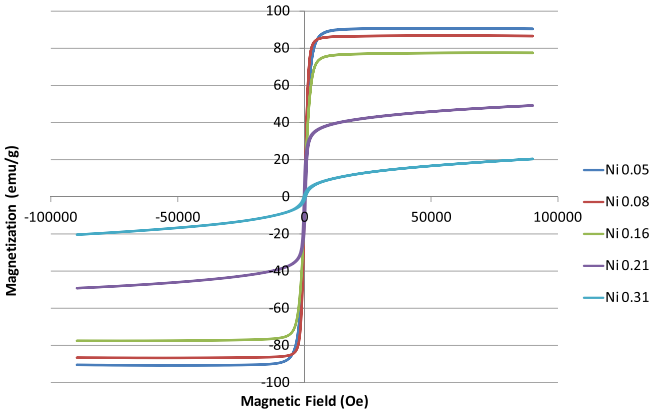

FIG. 5. Magnetization vs. magnetic field at 12 K for all Ni concentrations.

conjunction with the presence of a small amount of NiO. Our data are in agreement with that of Feng *et al.*[24] and suggest that the metal to insulator transition occurs over a finite temperature range between $x = 0.20$ and $x = 0.31$ and may also be associated with a change from charge ordering to antiferromagnetism. In the M_{ZFC} and M_{FC} curves for $x = 0.21$ and $x = 0.31$, there are long tails of magnetization that do not go to zero out to 300 K with $x = 0.21$ spanning more than 125 K while for $x = 0.31$ the transition spans approximately 50 K. For $x = 0.21$, these long magnetization tails are likely due to a combination of charge ordering, competition between the ferromagnetic couplings of Ni^{3+}-Mn^{3+} moments and the antiferromagnetic couplings of the Ni^{3+}-Mn^{4+} and Ni^{3+}-Ni^{3+} moments and a small effect from NiO. The amount of NiO for $x = 0.31$ is larger than for $x = 0.21$, but the $x = 0.31$ sample exhibits a smaller magnetic moment with a magnetic tail that spans a shorter temperature range. Therefore, although some of the magnetization tail may be attributed to the antiferromagnetic NiO, it is likely that the charge ordering and magnetic couplings have a larger influence.

The magnetizations versus magnetic field curves at 5 K are plotted in Figure 5. For $x = 0.05$, 0.08, and 0.16, the magnetization saturates to values of 90.8 emu/g, 86.7 emu/g, and 77.5 emu/g, respectively. However, for $x = 0.21$ and 0.31, maximum values of 49.29 emu/g and 20.42 emu/g are reached at a 9 T field without complete saturation. These differences are likely additional indicators for the transition from ferromagnetic to antiferromagnetic interactions. The separation between $x = 0.16$ and $x = 0.21$ is witness to the onset of charge ordering and the metal to insulator transition as discussed by Feng *et al.*,[24] whereas the separation between $x = 0.21$ and $x = 0.31$ is attributed to the onset of antiferromagnetic ordering. One should note that the magnetization versus magnetic field data for the $x = 0.31$ sample indicates a very small residual ferromagnetic component that is too small ($\sim$5 emu/g) to be observed in our neutron diffraction data.

IV. CONCLUSIONS

We have studied the structural and magnetic properties of the $La_{0.7}Sr_{0.3}Mn_{1-x}Ni_xO_3$ system and have presented a new model that clearly accounts for the ferromagnetic and doubled-unit cell intensities observed. Neutron-diffraction is the only experimental tool that can provide a direct measurement of magnetic structure, and to our knowledge, this is the first powder neutron-diffraction study of this system.

Using neutron diffraction, we find the following:

(1) All samples show a single perovskite phase and a small amount of a NiO impurity phase that increases with increasing Ni content.
(2) At low Ni concentrations the system orders ferromagnetically while at high Ni concentration the system orders antiferromagnetically. At intermediate compositions, the system shows charge ordering with a ferromagnetic ground state. For all compositions the neutron-diffraction data are fit with constant Ni^{3+}, Mn^{3+}, and Mn^{4+} moments, excluding the existence of spin glass or cluster glass behavior.
(3) The neutron-diffraction data clearly indicate that the antiferromagnetic coupling between Mn^{4+} and Ni^{3+} must be the driving force in this system.
(4) The nickel moments align antiferromagnetically to the ferromagnetically coupled Mn^{3+} and Mn^{4+} moments for $x < 0.31$. At $x = 0.31$, the antiferromagnetic coupling between Ni^{3+} and Mn^{4+} moments becomes dominant, leading to a long range antiferromagnetic state.
(5) The lattice parameters and unit cell volume decrease with increasing Ni content while the oxygen content remains stoichiometric within error tolerances, requiring the nickel ion to be Ni^{3+}.
(6) The magnetic unit cell for $x \geq 0.21$ consists of a doubled nuclear cell along the c-axis.
(7) The likely exchange mechanism for Ni^{3+}-$O^{2-}$$Mn^{3+}$ is double exchange where as for Ni^{3+}-$O^{2-}$$Mn^{4+}$ it is superexchange, accounting for the transition from charge ordering to antiferromagnetism as the Mn^{3+} concentration decreases.

Using magnetization measurements, we find the following:

(1) Competition between the ferromagnetic couplings of Ni^{3+}-Mn^{3+} moments and the antiferromagnetic couplings of Ni^{3+}-Mn^{4+} and Ni^{3+}-Ni^{3+} moments as evidenced by the long tails of magnetization in samples with higher Ni concentration and, antiferromagnetic-like behavior at lower temperatures.
(2) Evidence of the imminent onset of charge ordering and metal to insulator transition in the $x = 0.16$ sample from the broad ferromagnetic to paramagnetic transition, the separation between $x = 0.16$ and $x = 0.21$ magnetization and magnetic moments, and the temperature dependent M_{ZFC} and M_{FC} magnetization differences within the $x = 0.16$ sample.
(3) Agreement between our magnetic model derived from the neutron data with earlier studies of the dramatic change in magnetic behavior between $x = 0.16$ and $x = 0.21$ and between $x = 0.21$ and $x = 0.31$.

While magnetic measurements may leave some ambiguity about the nature of the low temperature state, the neutron-diffraction data clearly show that over a small range of composition, long range magnetism comprised of competing

ferromagnetic and antiferromagnetic interactions between Mn^{3+}, Mn^{4+}, and Ni^{3+} coupled with charge ordering leads to a doubled unit cell with a ferromagnetic ground state.

[1]G. H. Jonker and J. H. Van Santen, Physica **16**, 337–349, (1950).
[2]Myron B. Salamon and M. Jaime, Rev. Mod. Phys. **73**, 583 (2001).
[3]E. O. Wollan and W. C. Koehler, Phys. Rev. **100**, 545–563 (1955).
[4]J. B. Goodenough, *Magnetism and the Chemical Bond* (Krieger, Huntington, 1976).
[5]L. Brorovskikh, G. Mazo, and E. Kemnitz, Solid State Sci. **5**, 409–417 (2003).
[6]R. J. H. Voorhoeve, D. W. Johnson, J. P. Remeika, and P. K. Gallagher, Science **195**, 827–833 (1977).
[7]J. T. Vaughey, J. R. Mawdsley, and T. R. Krause, Mater. Res. Bull. **42**, 1963–1968 (2007).
[8]A. J. Millis, P. B. Littlewood, and B. I. Shraiman, Phys. Rev. Lett. **74**(25), 5144 (1995).
[9]A. J. Millis, Phys. Rev. B **53**, 8434 (1996).
[10]W. Archibald, J.-S. Zhou, and J. B. Goodenough, Phys. Rev. B **53**, 14445 (1996).
[11]C. Zener, Phys. Rev. **82**, 403–405 (1951).
[12]H. A. Kramers, Physica **1**, 182 (1934).
[13]H. A. Jahn and E. Teller, Proc. R. Soc. London, Ser. A **161**(905), 220 (1937).
[14]J. B. Goodenough and A. L. Loeb, Phys. Rev. **98**(2), 391 (1955).
[15]J. B. Goodenough, Phys. Rev. **100**(2), 564 (1955).
[16]T. Arima, Y. Tokura, and J. B. Torrance, Phys. Rev. B **48**, 17006 (1993).
[17]A. Urushibara, Y. Moritomo, T. Arima, A. Asamitsu, G. Kido, and Y. Tokura, Phys. Rev. B **51**, 14103 (1995).
[18]M. C. Martin, G. Shirane, Y. Endoh, K. Hirota, Y. Moritomo, and Y. Tokura, Phys. Rev. **53**(21), 14285–14290 (1996).
[19]Y. Tokura, A. Urushibara, Y. Moritomo, T. Arima, A. Asamitsu, G. Kido, and N. Furukawa, J. Phys. Soc. Jpn. **63**, 3931 (1994).
[20]A. Asamitsu, Y. Moritomo, Y. Tomioka, T. Arima, and Y. Tokura, Nature **373**, 407 (1995).
[21]H. Kuwahara, Y. Tomioka, A. Asamitsu, Y. Moritomo, and Y. Tokura, Science **270**, 961 (1995).
[22]L. M. Medarde, J. Phys.: Condens. Matter **9**, 1679 (1997).
[23]Z. H. Wang, J. W. Cai, B. G. Shen, X. Chen, and W. S. Zhan, J. Phys.: Condens. Matter **12**, 601 (2000).
[24]J.-W. Feng and L.-P. Hwang, Appl. Phys Lett. **75**(11), 1592 (1999).
[25]A. Wold, R. J. Arnott, and J. B. Goodenough, J. Appl. Phys. **29**, 387–389 (1958).
[26]R. D. Shannon, Acta Crystallogr., Sect. A: Cryst. Phys., Diffr., Theor. Gen. Crystallogr. **32**, 751 (1976).
[27]J. Rodriguez-Carvajal, FULLPROF 2K, Version 3.00, Laboratoire Leon Brillouin–JRC, 2004.
[28]Thomas F. Creel, Jinbo B. Yang, M. Kahveci, J. Lamsal, S. K. Malik, S. Quezado, B. W. Benapfl, H. Blackstead, O. A. Pringle, William B. Yelon, and William J. James, MRS Proc. **1327**, mrss11–1327-g08-02, doi:10.1557/opl.2011.852 (2011).
[29]H. Kawano, R. Kajimoto, M. Kubota, and H. Yoshizawa, Phys. Rev. B **53**(22), R14709 (1996).
[30]J. Hu, C. Ji, H. Qin, J. Chen, Y. Hao, and Y. Li, J. Magn. Magn. Mater. **241**, 271 (2002).
[31]Y. Tomioka, A. Asamitsu, Y. Moritomo, H. Kuwahara, and Y. Tokura, Phys. Rev. Lett. **74**(25), 5108 (1995).